9952 *Inorg. Chem.* **2009**, *48*, 9952–9957
DOI: 10.1021/ic9009652

Inorganic Chemistry
Article

Crystal Structures and Characterizations of Mixed Valence 12 L-Perovskites $Ba_4EuM_3O_{12}$ (M = Ru and Ir)

Yuki Shimoda, Yoshihiro Doi, Makoto Wakeshima,* and Yukio Hinatsu

Division of Chemistry, Graduate School of Science, Hokkaido University, Sapporo 060-0810, Japan

Received May 16, 2009

The crystal structures and characterizations of $Ba_4EuM_3O_{12}$ (M = Ru and Ir) are reported. They crystallize in a monoclinic 12-L-perovskite-type structure with space group *C*2/*m*. The M_3O_{12} trimers and EuO_6 octahedra are alternately linked by corner-sharing and form the perovskite-type structure with 12 layers. The ^{151}Eu Mössbauer and X-ray photoelectron spectra reveal that the Eu and M ions are in the trivalent and mixed valence (+4.33) oxidation states, respectively. Their electrical conductivities show semiconducting behavior with an activation energy of ~0.2 eV above room temperature and demonstrate two-dimensional Mott variable range hopping behavior at low temperatures. The magnetic susceptibility and specific heat measurements indicate that an antiferromagnetic ordering occurs at 4 K, which is due to the magnetic interaction between Ru_3O_{12} trimers. On the other hand, the Ir_3O_{12} trimer is found to be nonmagnetic.

Introduction

Perovskite-family oxides have attracted much interest due to their exotic electronic, magnetic, and structural properties. It is well-known that a perovskite ABO_3 with a tolerance factor less than 1.0 forms a three-dimensional frame network of corner-sharing BO_6 octahedra, which can be described as a stacking sequence *abc*... Perovskites with a tolerance factor (*t*) greater than unity form face-sharing BO_6 octahedra, and the stacking sequence varies with the value of *t*.[1]

If two kinds of cations are present in the B site, the ordering ratio of B and B′ cations increases with an increasing difference in charge and size between B and B′ cations. Most perovskites $BaLn_{1-x}M_xO_3$ containing both transition metal (M) and rare earth (Ln) ions exhibit a perfectly ordered B sublattice due to the difference in their ionic radii. The stacking sequence is controlled by changing the ratio of the Ln and M ions; that is, double perovskites Ba_2LnMO_6 have a 1:1-type B-site cation ordering with the sequence *abc*..,[2−6] and triple perovskites $Ba_3LnM_2O_9$ crystallize in a 6H-perovskite structure with a 1:2-type B-site cation ordering (the *abacbc*... sequence).[7,8] Quadruple perovskites $Ba_4LnMn_3O_{12-x}$ crystallize in a 12R-perovskite structure with a stacking sequence of *abcbcababcac*... which consists of a face-sharing Mn_3O_{12} trimer isolated by single LnO_6 octahedron layers.[9,10] These compounds often show magnetic orderings of the Ln and M ions, and the stacking sequence determines magnetic interaction paths.[11−19]

In our previous study,[20] new quadruple perovskites $Ba_4LnRu_3O_{12}$ were investigated, and their crystal structures were more distorted from rhombohedral (12R) to monoclinic (12M) by replacing the larger Ln ion.[20] Both $Ba_4PrRu_3O_{12}$ and $Ba_4TbRu_3O_{12}$, which contain tetravalent magnetic Ln

*Author to whom correspondence should be addressed. Phone and Fax: +81(0)11-706-2706. E-mail: wake@sci.hokudai.ac.jp.

(1) Müller, U. In *Inorganic Structural Chemistry*, 2nd ed.; Wiley: Chichester, U. K., 2006.
(2) Filipev, V. S.; Fesenko, E. G. *Kristallografiya* **1961**, *6*, 770.
(3) Filipev, V. S.; Fesenko, E. G. *Kristallografiya* **1965**, *10*, 626.
(4) Donohue, P. C.; McCann, E. L. *Mater. Res. Bull.* **1977**, *12*, 519.
(5) Thumm, I.; Treiber, U.; Kemmler-Sack, S. *J. Solid State Chem.* **1980**, *35*, 156.
(6) Treiber, U.; Kemmler-Sack, S. *Z. Anorg. Allg. Chem.* **1981**, *478*, 223.
(7) Treiber, U.; Kemmler-Sack, S.; Ehmann, A.; Schaller, H. U.; Duerrschmidt, E.; Thumm, I.; Bader, H. *Z. Anorg. Allg. Chem.* **1981**, *481*, 143.
(8) Thumm, I.; Treiber, U.; Kemmler-Sack, S. *J. Solid State Chem.* **1980**, *35*, 156.
(9) Fuentes, A. F.; Boulahya, K.; Amador, U. *J. Solid State Chem.* **2004**, *177*, 714.
(10) Kuang, X.; Craig, B.; Allix, M.; Claridge, J. B.; Hughes, H.; Rosseinsky, M. J. *Chem. Mater.* **2006**, *18*, 5130.
(11) Battle, P. D.; Goodenough, J. B.; Price, R. *J. Solid State Chem.* **1983**, *46*, 234.
(12) Izumiyama, Y.; Doi, Y.; Wakeshima, M.; Hinatsu, Y.; Oikawa, K.; Shimojo, Y.; Morii, Y. *J. Mater. Chem.* **2000**, *10*, 2364.
(13) Wakeshima, M.; Harada, D.; Hinatsu, Y. *J. Mater. Chem.* **2000**, *10*, 419.
(14) Izumiyama, Y.; Doi, Y.; Wakeshima, M.; Hinatsu, Y.; Shimojo, Y.; Morii, Y. *J. Phys.: Condens. Matter* **2001**, *13*, 1303.
(15) Wakeshima, M.; Izumiyama, Y.; Doi, Y.; Hinatsu, Y. *Solid State Commun.* **2001**, *120*, 273.
(16) Cussen, E. J.; Lynham, D. R.; Rogers, J. *Chem. Mater.* **2006**, *18*, 2855.
(17) Doi, Y.; Hinatsu, Y.; Shimojo, Y.; Ishii, Y. *J. Solid State Chem.* **2001**, *161*, 113.
(18) Doi, Y.; Wakeshima, M.; Hinatsu, Y.; Tobo, A.; Ohoyama, K.; Yamaguchi, Y. *J. Mater. Chem.* **2001**, *11*, 3135.
(19) Lufaso, M. W.; zur Loye, H.-C. *Inorg. Chem.* **2005**, *44*, 9143.
(20) Shimoda, Y.; Doi, Y.; Hinatsu, Y.; Ohoyama, K. *Chem. Mater.* **2008**, *20*, 4512.

 Published on Web 09/21/2009

ions, show an antiferromagnetic ordering, while $Ba_4CeRu_3O_{12}$ is paramagnetic down to 1.8 K due to the nonmagnetic ground state ($J = 0$) of the Ru_3O_{12} trimer[21] and the Ce^{4+} ion. For these $Ba_4LnRu_3O_{12}$ (Ln = Ce, Pr, Tb) compounds, the Ru ion is in the tetravalent state in the Ru_3O_{12} trimer. On the other hand, physical properties of $Ba_4LnRu_3O_{12}$ containing trivalent Ln and mixed-valence Ru ions have not been investigated yet, although mixed-valence Ru oxides often exhibit interesting electrical and magnetic properties.[22−24]

We focus our attention on the electronic properties of $Ba_4EuM_3O_{12}$ (M = Ru, Ir). Understanding the electronic state of the M_3O_{12} trimer in these compounds will be easy because the Eu^{3+} ion adopts a nonmagnetic ground state ($J = 0$). In this paper, we report a new synthesis of $Ba_4EuIr_3O_{12}$ and the electrical and magnetic properties of $Ba_4EuM_3O_{12}$ (M = Ru, Ir).

Experimental Section

Polycrystalline samples of $Ba_4EuIr_3O_{12}$ were prepared using a standard solid-state reaction. $BaIrO_3$, BaO, BaO_2, and Eu_2O_3 were weighed out in a stoichiometric ratio and well mixed in an agate mortar. Due to the easy sublimation of Ba and Ir oxides, excess amounts (~5 mol %) of $BaIrO_3$ were added. The mixtures were pressed into pellets and enclosed with platinum tubes, and then they were sealed in evacuated silica tubes. They were heated at 1250 °C for 36 h. The method to synthesize $Ba_4EuRu_3O_{12}$ has been described elsewhere.[20] The samples for the electrical resistivity measurements were pelletized and then sintered at 1100 °C for 36 h.

Powder X-ray diffraction (XRD) data were collected in the range $10° \le 2\theta \le 120°$ using a 2θ step size of 0.02° with Cu Kα radiation monochromatized with curved graphite on a Rigaku MultiFlex diffractometer. Crystal structures were determined using the Rietveld technique with the program RIETAN-FP.[25]

The ^{151}Eu Mössbauer spectrum was measured with a conventional Mössbauer VT-6000 (Laboratory Equipment Co., Japan) transmission spectrometer at room temperature. The spectrometer was calibrated using α-iron at room temperature, and the isomer shift was determined relative to the shift ($\delta = -0.03$ mm/s) of europium trifluoride (EuF_3).

The X-ray photoelectron spectrum was measured with an X-ray photoelectron spectrometer (XPS) JPS-9200 (JEOL). The Al Kα X-ray source was used for performing full and narrow scans. The full scan and core-level spectra were recorded in steps of 1 and 0.1 eV, respectively.

The temperature dependence of the resistivity was measured by the dc four-probe technique in a temperature range of 60−1000 K. The sample was sintered and then cut into a piece approximately 1 mm × 1.5 mm × 3 mm in size.

Magnetic susceptibility measurements were carried out with a SQUID magnetometer (Quantum Design, MPMS-5S). The temperature dependence of the magnetic susceptibilities was measured under both zero-field-cooled (ZFC) and field-cooled (FC) conditions in an applied field of 0.1 T over the temperature range between 1.8 and 400 K.

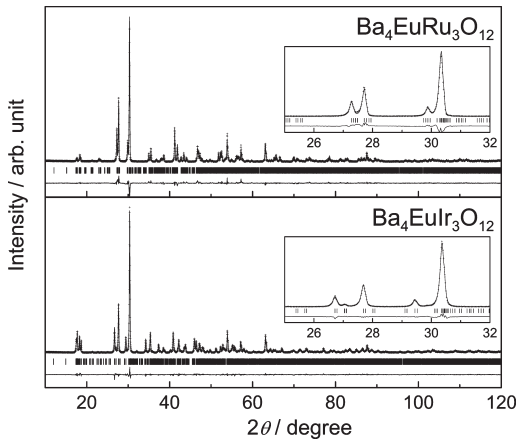

Figure 1. X-ray diffraction profiles for $Ba_4EuRu_3O_{12}$ and $Ba_4EuIr_3O_{12}$. The inset shows the XRD profile in the range $25° \le 2\theta \le 32°$.

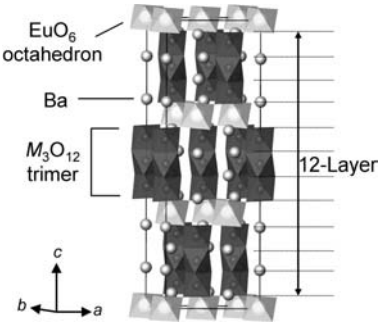

Figure 2. Crystal structure of $Ba_4EuM_3O_{12}$ (M = Ru, Ir) with a monoclinic unit cell.

Specific heat measurements were performed using a relaxation technique with a heat capacity measurement system (Quantum Design, PPMS model) in the temperature range of 1.8−300 K. The pelletized sample was mounted on a thin alumina plate with Apiezon N grease for better thermal contact.

Results and Discussion

Crystal Structure and Oxidation States. Figure 1a,b show the powder XRD patterns for $Ba_4EuRu_3O_{12}$ and $Ba_4EuIr_3O_{12}$, respectively. Both patterns were indexed with a monoclinic 12-L-perovskite-type cell with space group $C2/m$. The Rietveld analysis was performed with the program RIETAN-FP.[25] The atomic positional and displacement parameters of $Ba_4PrRu_3O_{12}$, which were determined through the neutron diffraction measurements,[20] are used as the initial parameters. Structural parameters were summarized in Tables S1 and S2 (Supporting Information). The crystal structure of $Ba_4EuIr_3O_{12}$ is more distorted than that of $Ba_4EuRu_3O_{12}$.

Figure 2 illustrates the monoclinic 12-L-perovskite-type structure of $Ba_4EuM_3O_{12}$ (M = Ru, Ir). In this structure, M ions are octahedrally coordinated by six oxide ions, and three MO_6 octahedra share faces forming a M_3O_{12} trimer. The M−M interatomic distances in the M_3O_{12} trimer are r(Ru−Ru) = 2.4−2.6 Å for $Ba_4EuRu_3O_{12}$ and r(Ir−Ir) = 2.5−2.6 Å for $Ba_4EuIr_3O_{12}$. These distances are close to those of the triple perovskites $Ba_3M'M_2O_9$ (M′ = trivalent cation; M = Ru, Ir) with the M_2O_9 dimer in which the M ion is in the +4.5 oxidation state.[19] The

(21) Drillon, M.; Padel, L.; Bernier, J. C. *J. Chem. Soc., Faraday Trans. 2* **1979**, *75*, 1193.
(22) Khalifah, P.; Nelson, K. D.; Jin, R.; Mao, Z. Q.; Liu, Y.; Huang, Q.; Gao, X. P. A.; Ramirez, A. P.; Cava, R. J. *Nature* **2001**, *411*, 669.
(23) Stitzer, K. E.; Smith, M. D.; Gemmill, W. R.; zur Loye, H.-C. *J. Am. Chem. Soc.* **2002**, *124*, 13877.
(24) Mao, Z. Q.; Rosario, M. M.; Nelson, K. D.; Okuno, D.; Ueland, B.; Deac, I. G.; Schiffer, P.; Liu, Y.; Cava, R. J. *Phys. Rev. Lett.* **2003**, *90*, 186601.
(25) Izumi, F.; Momma, K. *Solid State Phenom.* **2007**, *130*, 15.

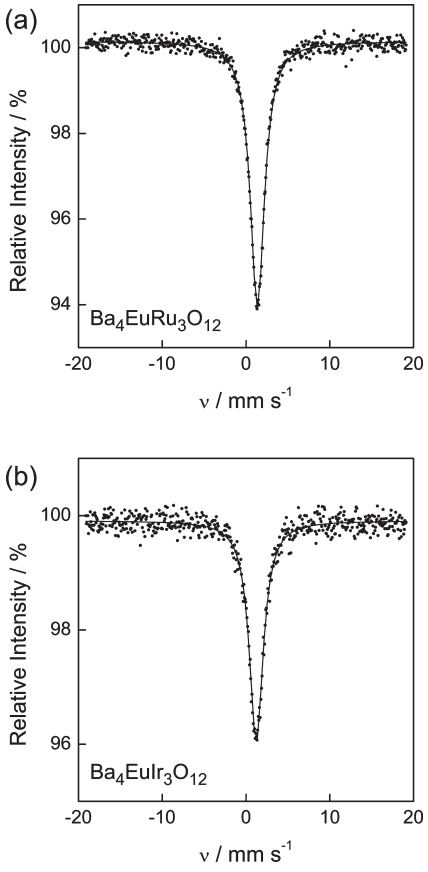

Figure 3. ^{151}Mössbauer spectra of (a) $Ba_4EuRu_3O_{12}$ and (b) $Ba_4EuIr_3O_{12}$.

M_3O_{12} trimers and EuO_6 octahedra are alternately linked by corner-sharing and form the perovskite-type structure with 12 layers (the stacking sequence: *abcbcababcac*...[26]).

The average Eu−O bond lengths for $Ba_4EuRu_3O_{12}$ and $Ba_4EuIr_3O_{12}$ are 2.33 and 2.27 Å, respectively, and are closer to the value for $Eu^{3+}-O^{2-}$ (2.35 Å) than that for $Eu^{2+}-O^{2-}$ (2.57 Å), which are calculated from Shannon's ionic radii.[27] In order to determine oxidation states of the Eu ions, the ^{151}Eu Mössbauer spectra of $Ba_4EuM_3O_{12}$ were measured at room temperature, and they are shown in Figure 3a,b. Since the Eu 2*d* and 4*i* sites in $Ba_4EuM_3O_{12}$ have an octahedral point symmetry with a monoclinic distortion, an electric field gradient tensor exists. Due to the distortion by the quadrupole interaction, each absorption peak should be fitted with 12 Lorentzian lines. To simplify this analysis, the overlapped peaks of Eu^{3+} were fitted with a single Lorentzian. The isomer shifts δ for $Ba_4EuRu_3O_{12}$ and $Ba_4EuIr_3O_{12}$ are determined to be 1.35 and 1.22 mm/s, respectively, which reveals that the Eu ions are in the trivalent state in both compounds.

From the chemical formula, one expects that the M ions in $Ba_4EuM_3O_{12}$ are in a mixed-valence state and that its average oxidation state is +4.33. The XPS measurements of $Ba_4EuM_3O_{12}$ were carried out to elucidate electronic states of the mixed-valence M_3O_{12} trimers. Figure 4a,b show the XPS spectra of Ru 3d and Ir 4f, respectively. The spectra of $BaMO_3$ and Ba_2EuMO_6, which contain the M^{4+} and M^{5+} ions, respectively, are also plotted as references.

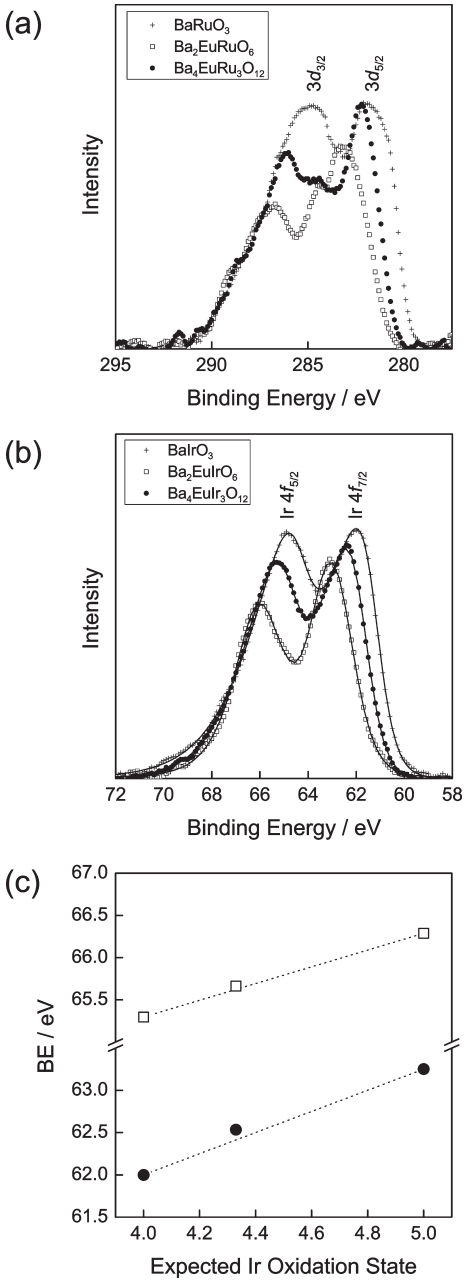

Figure 4. XPS spectra of (a) $Ba_4EuRu_3O_{12}$ and (b) $Ba_4EuIr_3O_{12}$. The XPS spectra of $BaMO_3$ and Ba_2EuMO_6 are also plotted in each part. (c) Binding energies of the $4f_{7/2}$ and $4f_{5/2}$ orbitals of the Ir ions are plotted as a function of the expected Ir oxidation state.

All spectra for the Ru compounds have two peaks of Ru $3d_{5/2}$ and $3d_{3/2}$, as shown in Figure 4a. A shoulder is observed around 284.5 eV between two Ru 3d peaks for $Ba_4EuRu_3O_{12}$ and Ba_2EuRuO_6, and the $3d_{3/2}$ peak is broader for $BaRuO_3$. Because the C 1s peaks in XPS often include signals due to impurities, these shoulders should be attributable to C 1s peaks. The Ru $3d_{5/2}$ and $3d_{3/2}$ peaks of $BaRuO_3$, $Ba_4EuRu_3O_{12}$, and Ba_2EuRuO_6 shift toward a higher binding energy (BE), which suggests that the Ru ions of $Ba_4EuRu_3O_{12}$ are in the intermediate state between the +4 and +5 oxidation states.

Two peaks of Ir $4f_{7/2}$ and $4f_{5/2}$ are observed in all of the spectra, as shown in Figure 4b, and these peaks of $BaIrO_3$, $Ba_4EuIr_3O_{12}$, and Ba_2EuIrO_6 shift toward a higher BE.

(26) Longo, J. M.; Kafalas, J. A. *J. Solid State Chem.* **1969**, *1*, 103–108.
(27) Shannon, R. D. *Acta Crystallogr., Sect. A* **1976**, *32*, 751–767.

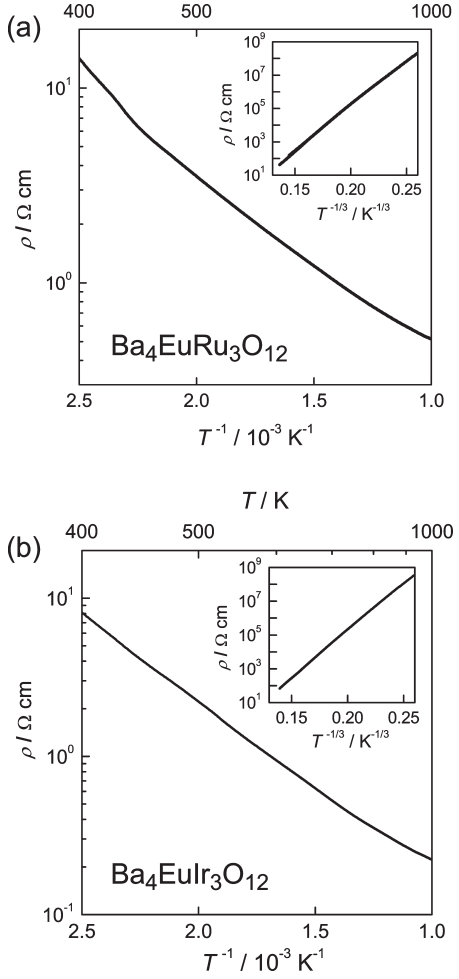

Figure 5. Temperature dependence of the resistivity (ρ) for (a) $Ba_4EuRu_3O_{12}$ and (b) $Ba_4EuIr_3O_{12}$. The insets show the log $\rho - T^{-1/3}$ plot of each compound.

The BEs of the $4f_{7/2}$ and $4f_{5/2}$ peaks are determined to be 62.0 and 65.7 eV for $BaIrO_3$, 62.5 and 66.3 eV for $Ba_4EuIr_3O_{12}$, and 63.3 and 66.3 eV for Ba_2EuIrO_6, respectively, using an asymmetric peak function,[28] and these BE values are plotted against the expected Ir oxidation state in Figure 4c. The BE values reveal that the Ir ions of $Ba_4EuIr_3O_{12}$ are not in the +4 and +5 oxidation states with a charge separation but in the +4.33 oxidation state in the Ir_3O_{12} trimers.

Electrical Conductivity. Figure 5 shows the temperature dependences of the electrical resistivities (ρ) of $Ba_4EuM_3O_{12}$ (M = Ru, Ir). Both compounds exhibit a thermally activated conductivity up to 1000 K, but the temperature dependence demonstrates different behaviors below and above room temperature.

The temperature dependences below room temperature do not follow the Arrhenius law (log $\rho \propto T^{-1}$). Below 300 K, log ρ is proportional to $T^{-1/d+1}$ with $d = 2$, as shown in the insets of Figure 5a,b. These temperature dependences are typical for Mott variable-range hopping (VRH) conduction of localized carriers in two dimension systems.[29] This resistivity behavior is often shown in six-L-perovskites; for example, the log ρ of 6H-perovskite $Ba_3EuRu_2O_9$ containing Ru_2O_9 dimers is proportional to $T^{-1/3}$ below 400 K.[18]

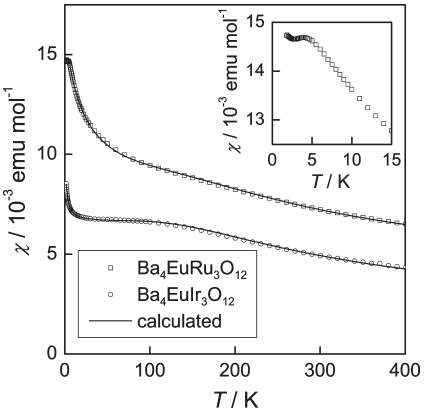

Figure 6. Temperature dependence of the magnetic susceptibility (χ) for $Ba_4EuRu_3O_{12}$ (M = Ru, Ir). The inset shows the $\chi - T$ plot of $Ba_4EuRu_3O_{12}$ below 15 K.

On the other hand, above room temperature, the temperature dependences follow the Arrhenius law, and the activation energies (E_a) are estimated be 0.18 eV for $Ba_4EuRu_3O_{12}$ and 0.22 eV for $Ba_4EuIr_3O_{12}$ from the relation $\rho = \rho_0 \exp(E_a/k_BT)$ in the temperature range from 500 to 900 K. These values are comparable with E_a (0.23 eV) of the double-perovskite Ba_2EuIrO_6 in the temperature range 300−750 K.[30]

In $Ba_4EuM_3O_{12}$, the EuO_6 octahedra are isolated from each other, each linking to M_3O_{12} trimers into a three-dimensional sublattice. A M−O−Eu−O−M conduction path should play a key role in the conduction mechanism of $Ba_4EuM_3O_{12}$. For more detailed discussion about the semiconducting and two-dimensional VRH conduction mechanism, it is necessary to measure the resistivity using a single crystal.

Magnetic Susceptibility and Specific Heat. Figure 6 shows the temperature dependence of the magnetic susceptibility (χ) for $Ba_4EuM_3O_{12}$. These susceptibilities do not obey the Curie−Weiss law, as shown in Figure S1 (Supporting Information). For $Ba_4EuIr_3O_{12}$, no anomaly is observed down to 1.8 K. The molar paramagnetic susceptibility of $Ba_4EuIr_3O_{12}$ is given by

$$\chi = \chi(Eu^{3+}) + \chi(Ir_3O_{12}\text{trimer}) + \chi_{TIP} \quad (1)$$

where χ_{TIP} is the temperature-independent term containing the diamagnetic term. The susceptibility plateau below 100 K is attributable to the temperature-independent term of the Van Vleck formula by the population of the nonmagnetic ground state ($^7F_0$) for the Eu^{3+} ion. Considering the contribution of the excited states ^7F_J ($J = 1, 2, ..., 6$), the molar magnetic susceptibility of Eu^{3+} can be written by the following equation:

$$\chi(Eu^{3+}) = \frac{N_A\mu_B{}^2/3k_B}{\gamma T} \frac{24+(13.5\gamma-1.5)\,e^{-\gamma}+(67.5\gamma-2.5)\,e^{-3\gamma}+(189\gamma-3.5)\,e^{-6\gamma}+...}{1+3\,e^{-\gamma}+5\,e^{-3\gamma}+7\,e^{-6\gamma}+...} \quad (2)$$

(28) Doniach, S.; Sunjic, M. *J. Phys. C* **1970**, *3*, 285.
(29) Mott, N. F.; Davis, E. A. *Electronic Processes in Non-Crystalline Materials*, 2nd ed.; Clarendon Press: Oxford, U. K., 1979.
(30) Ramos, E. M.; Alvarez, I.; Viega, M. L.; Pico, C. *J. Mater. Sci. Lett.* **1995**, *14*, 1577.

where $\gamma = \lambda/k_BT$ is 1/21 of the ratio of the overall multiplet width to k_BT.[31] To analyze the susceptibilities of the Ir_3O_{12} trimer, we attempted to apply the susceptibility of the trinuclear cluster models to the experimental data, but the fitting results were unsatisfactory. The best fitting result was obtained using the simple Curie−Weiss (CW) law. Then, eq 1 was replaced by the following relation:

$$\chi = \chi(Eu^{3+}) + C/(T - \Theta_w) + \chi_{TIP} \quad (3)$$

By fitting eq 3 to the experimental magnetic susceptibility, the spin−orbit coupling constant λ of Eu^{3+}, the Curie constant C, and the Weiss constant Θ_W are obtained and determind to be $\lambda = 332(3)\ cm^{-1}$, $C = 5.00(7) \times 10^{-3}$ emu K/mol, and $\Theta_W = -0.77(3)$ K. This value of C is considerably smaller than that of the theoretical value (0.375 emu/mol) for a localized electron system with $S = 1/2$, which means that the CW behavior below 20 K is due to a tiny amount of paramagnetic impurities. It is suggested that the ground state of the Ir_3O_{12} trimer is nonmagnetic.

The molar paramagnetic susceptibility of $Ba_4EuRu_3O_{12}$ is also given by $\chi = \chi(Eu^{3+}) + C/(T - \Theta_W) + \chi_{TIP}$. By fitting this equation to the experimental data, λ, C, and Θ_W are obtained and determined to be 366(3) cm^{-1}, 0.174(3) emu/mol, and −21.0(5) K, respectively. From the C value of 0.174 emu K/mol, the effective magnetic moment μ_{eff} is calculated to be 1.18 μ_B and is ~70% of that (1.73 μ_B) of a spin-half system ($S = 1/2$). The large negative Θ_W indicates that the magnetic interaction between the Ru_3O_{12} trimers is antiferromagnetic. As shown in the inset of Figure 6, an antiferromagnetic transition is observed around 4 K with no divergence between the ZFC and FC susceptibilities.

Figure 7a shows the temperature dependence of the specific heat of $Ba_4EuRu_3O_{12}$. A broad peak is observed around 4 K, corresponding to the anomaly found in the magnetic susceptibilities, which indicates the existence of an antiferromagnetic ordering at this temperature. The specific heat of semiconducting $Ba_4EuRu_3O_{12}$ consists of a magnetic contribution (C_{mag}) and a lattice contribution (C_{lat}). The C_{lat} is represented by the usual harmonic lattice series in odd powers of T:

$$C_{lat} = B_3T^3 + B_5T^5 + B_7T^7 + \quad ... \quad (4)$$

For the Eu^{3+} ion of $Ba_4EuRu_3O_{12}$, the energy difference between the nonmagnetic ground state ($J = 0$) and the first excited state ($J = 1$) is 366 cm^{-1} (527 K). On the assumption that the C_{mag} contribution is negligible in the temperature range from 20 to 25 K, the constants B_3, B_5, and B_7 were determined by fitting eq 4 to the observed specific heat data between 20 and 25 K. The C_{mag} is obtained by subtracting C_{lat} from the total C_p. A dashed line in the $C_p - T$ curve below 1.8 K represents the extrapolated specific heat. This is calculated by using the equation $C_p = AT^3 + C_{lat}$ in the temperature range 1.8 K ≤ T ≤ 2.2 K, because C_{mag} for an antiferromagnetic state is proportional to T^3.[32] The temperature dependence

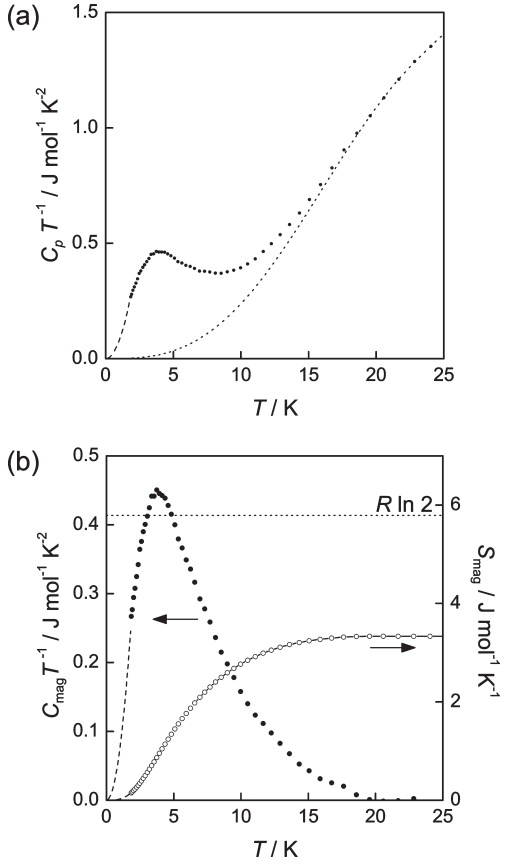

Figure 7. Temperature dependence of (a) the specific heat and (b) the magnetic specific heat and the magnetic entropy for $Ba_4EuRu_3O_{12}$.

of the C_{mag}/T and the magnetic entropy calculated by $S_{mag} = \int (C_{mag}/T)\, dT$ are shown in Figure 7b. From the $S_{mag} - T$ curve, the magnetic entropy change is estimated to be 3.3 J mol^{-1} K^{-1} at 20 K, and this value is ~60% of the $S = 1/2$ value of R ln 2 (5.76 J/mol K). The magnetic susceptibility and specific heat of $Ba_4EuRu_3O_{12}$ reveal that the Ru_3O_{12} trimer has localized spins which are smaller than $S = 1/2$, and that a long-range antiferromagnetic ordering occurs at 4 K. In our previous study,[20] $Ba_4PrRu_3O_{12}$ and $Ba_4TbRu_3O_{12}$ showed an antiferromagnetic ordering through the magnetic interaction path of Ru−O−Pr(Tb)−O−Ru including magnetic Pr^{4+} ($^2F_{5/2}$) and Tb^{4+} ($^8S_{7/2}$) ions. On the other hand, for $Ba_4EuRu_3O_{12}$, the ground state of the trivalent Eu ion is nonmagnetic. Consequently, it is considered that the magnetic interaction path (Ru−O−O−Ru) between the Ru_3O_{12} trimers plays an important role in the long-range ordering.

Molecular Orbitals of M_3O_{12} Trimer. For mixed-valence compounds, Robin and Day proposed the following classifications:[33]

Class I: Unpaired electrons are localized

Class II: An intermediate state between classes I and III

Class III: Unpaired electrons are delocalized (IIIA, multinuclear complex; IIIB, solid with infinite delocalized electrons)

An insulating mixed-valence compound is divided into classes I and IIIA. In the case of class I, unpaired

(31) Van Vleck, J. H. *Theory of Electric and Magnetic Susceptibilities*; Clarendon Press: Oxford: U. K., 1932.

(32) Van Kranendonk, J.; Van Vleck, J. H. *Rev. Mod. Phys.* **1958**, *30*, 1.

(33) Robin, M. B.; Day, P. *Adv. Inorg. Chem. Radiochem.* **1967**, *10*, 247.

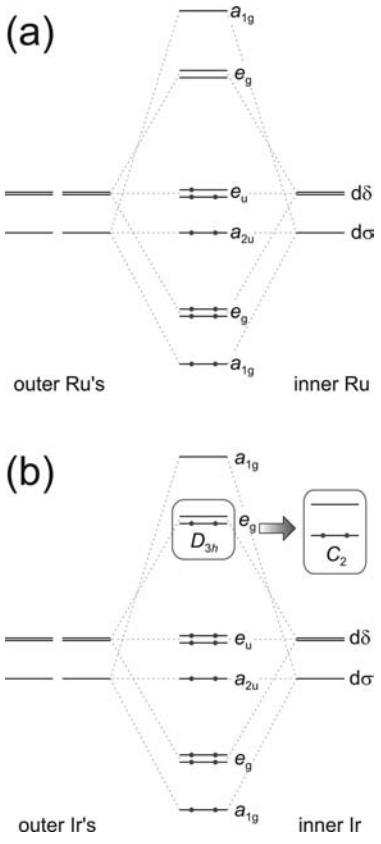

Figure 8. Qualitative molecular orbital diagram for M_3O_{12} trimer calculated by Bursten et al.[35] This figure shows only the "t_{2g}"-type transition metal d orbitals of (a) Ru_3O_{12} and (b) Ir_3O_{12} trimers.

electrons show a charge separation; that is, the M ions in $Ba_4EuM_3O_{12}$ have both the +4 and +5 oxidation states. However, it is apparent from their XPS spectra that the M ions of $Ba_4EuM_3O_{12}$ are in the +4.33 oxidation state without a charge separation. It is considered that $Ba_4EuM_3O_{12}$ belongs in class IIIA and that the M_3O_{12} trimer is a trinuclear unit isolated by the EuO_6 octahedron.

From the short M−M interatomic distances in the M_3O_{12} trimer, the O 2p and Ru 4d (or Ir 5d) orbitals are expected to form molecular orbitals in the M_3O_{12} trimer. If one considers the M_3O_{12} trimer as a magnetically isolated cluster, the susceptibilities can be modeled with the single spin subunit. The electronic structure of Ru_3Cl_{12} with a D_{3h} point symmetry has been described in several reports.[34−36] The energy scheme in M_3O_{12} of $Ba_4EuM_3O_{12}$ should be similar, but the degenerated energy levels are expected to be split into more levels due to the monoclinic distortion of the M_3O_{12} trimers and to the spin−orbit coupling of the 4d (5d) electrons.

The Ru_3O_{12} and Ir_3O_{12} trimers have 11 and 14 metal-based electrons, respectively. From Figure 8a, the electronic configuration of the Ru_3O_{12} trimer with D_{3h} point symmetry is $(a_{1g})^2(e_g)^4(a_{2u})^2(e_u)^3$. The highest occupied e_u orbitals (doublet) should be split into two singlets due to the monoclinic distortion and to the spin−orbit coupling, and thus the HOMOs have the $S = 1/2$ state. The experimental results can be understood on the basis of this model. The smaller μ_{eff} (1.18 μ_B) and S_{mag} (~3 J mol^{-1} K^{-1}) as compared with those of the $S = 1/2$ state should be attributable to an effect of covalency between the Ru and O ions.

The Ir_3O_{12} trimer has an electronic configuration of $(a_{1g})^2(e_g)^4(a_{2u})^2(e_u)^4(e_g)^2$. If a HOMO level is 2-fold degenerated, the ground state has two unpaired electrons in the e_g orbita; thus, the total spin is $S = 1$. This model is inconsistent with the $S = 0$ state of the nonmagnetic Ir_3O_{12} trimer. It is considered that the highest-occupied e_g orbitals are split into two singlets due to the monoclinic distortion of the Ir_3O_{12} trimer and to the spin−orbit coupling of the Ir 5d electrons, which causes the $S = 0$ state of the filled HOMO as shown Figure 8b.

Conclusion

We have reported the crystal structures and electronic properties of $Ba_4EuM_3O_{12}$ (M = Ru and Ir). They crystallize in a monoclinic 12-L-perovskite-type structure with space group $C2/m$. The M_3O_{12} trimers and EuO_6 octahedra are alternately linked by corner-sharing and form the perovskite-type structure with 12 layers. Through the XPS spectrum, electrical resistivity, and magnetic susceptibility measurements of both compounds, it is revealed that the M ion is in the mixed valence (+4.33) oxidation states of class IIIA. An antiferromagnetic ordering occurs at 4 K for $Ba_4EuRu_3O_{12}$, while the Ir_3O_{12} trimer in $Ba_4EuIr_3O_{12}$ is nonmagnetic. The difference in the magnetic behavior between $Ba_4EuRu_3O_{12}$ and $Ba_4EuIr_3O_{12}$ can be accounted for by the molecular orbitals of the M_3O_{12} trimers.

Supporting Information Available: Additional figures and tables. This material is available free of charge via the Internet at http://pubs.acs.org.

(34) Bino, A.; Cotton, F. A. *J. Am. Chem. Soc.* **1980**, *102*, 608.
(35) Bursten, B. E.; Cotton, F. A.; Fang, A. *Inorg. Chem.* **1983**, *22*, 2127.
(36) Gönen, Z. S.; Gopalakrishnan, J.; Eichhorn, B. W.; Greene, R. L. *Inorg. Chem.* **2001**, *40*, 4996.